

On the Detectability of Galactic Dark Matter Annihilation into Monochromatic Gamma-rays

Zhi-Cheng TANG,* Qiang YUAN, Xiao-Jun BI, and Guo-Ming CHEN
Institute of High Energy Physics, Chinese Academy of Sciences

Monochromatic γ -rays are thought to be the smoking gun signal for identifying the dark matter annihilation. However, the flux of monochromatic γ -rays is usually suppressed by the virtual quantum effects since dark matter should be neutral and does not couple with γ -rays directly. In the work we study the detection strategy of the monochromatic γ -rays in a future space-based detector. The monochromatic γ -ray flux is calculated by assuming supersymmetric neutralino as a typical dark matter candidate. We discuss both the detection focusing on the Galactic center and in a scan mode which detects γ -rays from the whole Galactic halo are compared. The detector performance for the purpose of monochromatic γ -rays detection, with different energy and angular resolution, field of view, background rejection efficiencies, is carefully studied with both analytical and fast Monte-Carlo method.

PACS numbers: 95.35.+d, 98.35.-a, 98.35.Gi

I. INTRODUCTION

The existence of dark matter (DM) in the Universe is widely accepted nowadays. The evidences come from many astronomical observations, which observed the gravitational effects of dark matter in different spatial scales, from dwarf galaxies, galaxies, galaxy clusters to the cosmological scale. It is recognized that DM particle should be neutral, cold and non-baryonic, which can only exist in theories beyond the standard model of particle physics. Among the large amount of DM candidates proposed in the literature, the weakly interacting massive particles (WIMP) are the most favored one, which can account for the observed DM density naturally.

In order to determine the nature of the WIMP DM particles, we generally have three ways to probe the interaction between DM particles and the standard particles: the direct detection measures the scattering by DM with the detector nuclei; or produce DM particles directly in a powerful collider such as LHC or ILC; finally the indirect detection searches for the DM annihilation or decay products in cosmic rays (CRs), including gamma-rays, electrons, positrons, protons, antiprotons and neutrinos. For indirect detection the gamma-rays are usually the best probe of DM because they are not deflected by the magnetic field during the propagation. Further the technology of high energy gamma ray detector was developed very fast in the last years. In general the gamma-rays are produced through the hadronization and decay of the DM annihilation/decay final states, and have continuous energy spectra. Since there are large diffuse backgrounds of gamma-rays, it is usually not easy to figure out the DM signals from the background. Another annihilation channel is to monochromatic gamma-rays with small branching ratio via loop diagram. The monochromatic gamma-rays by DM annihilation are usually taken

as the smoking-gun of the DM signal since there are no such background from astrophysical processes. If the detector has very good energy resolution, the background will be suppressed and the detectability will be improved.

In this work we discuss DM annihilation into monochromatic photons, $\chi_0\chi_0 \rightarrow \gamma\gamma$ and $\chi_0\chi_0 \rightarrow \gamma Z_0$, with energy of the gamma-ray photon m_χ and $m_\chi - m_Z^2/4m_\chi$ respectively. Here we neglect the kinetic energy of DM particles since its movement is non-relativistic today. For very massive DM $m_\chi \gg m_Z$, the photon energy of the two channels are identical and can not be distinguished in experiments. This work tries to give the perspective of detecting such line spectrum gamma-rays from DM annihilation in the Milky Way, and show the requirements for detector design.

The γ -ray flux from DM annihilation is proportional to the annihilation cross section and DM density square. As a typical WIMP DM we consider the lightest neutralino in the minimal supersymmetric standard model (MSSM) as an explicit example in our calculation. The cross section can be computed given the MSSM model parameters. In this work we will employ DarkSUSY package [1] to scan the MSSM parameter space. As to the Galactic DM density profile, numerical simulations indicate that DM is highly concentrated in the halo center. Therefore the Galactic center (GC) is usually the first choice searching for DM signals. In addition, there are also a large amount of substructures existing in the halo, mostly in the outer part of the halo. The contribution from substructures will also be discussed. The backgrounds for the monochromatic photon detection include CR nuclei (mainly protons and Helium for energies $\lesssim 10$ TeV), electrons, diffuse continuous γ -rays and the γ -ray point sources in the GC region. The nuclei and electrons can be rejected through the particle identification technique of the detector. For the diffuse γ -ray background we need a high energy resolution to suppress the background.

The paper is organized as follow. The MSSM model and the Galactic DM density distribution will be presented in Sec. II. In Sec. III the possible backgrounds

*Electronic address: tangzhch@ihep.ac.cn

in our study are introduced, especially those in the GC region. Sec. IV gives the results of detection sensitivity for the GC region through simple analytical estimate. We show in Sec. V the sensitivity for all-sky observation in the scan mode, with substructures included, using Monte-Carlo simulation. Finally we draw the conclusion and discussion in Sec. VI.

II. DARK MATTER ANNIHILATION INTO MONOCHROMATIC GAMMA-RAYS

The γ -ray flux from DM annihilation can be written as

$$\phi(\psi) = \frac{\rho_\odot^2 R_\odot}{4\pi} \times \frac{N\langle\sigma v\rangle}{2m_\chi^2} \times J(\psi), \quad (1)$$

where ψ is a specified direction away from the Galactic center, $\rho_\odot \approx 0.4 \text{ GeV cm}^{-3}$ [2, 3] is the local DM density, $R_\odot \approx 8.5 \text{ kpc}$ is the distance from the Earth to the GC, m_χ is the mass of DM particle, $\langle\sigma v\rangle$ is the velocity weighted thermal average annihilation cross section, the multiplicity $N = 1, 2$ for γZ_0 and $\gamma\gamma$ channels respectively. Finally $J(\psi)$ is the line-of-sight integral of the density square $J(\psi) = \frac{1}{\rho_\odot^2 R_\odot} \int \rho^2(l) dl$. The γ -ray flux depends on both the particle parameters and the density distribution of DM.

A. MSSM dark matter model

Without losing the generality we take neutralino in MSSM as a typical WIMP DM in this work. In order to reduce the number of free parameters in MSSM we only take a few relevant parameters to our discussion free, as done in Ref. [1], that is,

$$\mu, M_2, M_1, \tan\beta, M_A, m_0, A_b, A_t, \quad (2)$$

where μ is the Higgsino mass parameter, M_2 and M_1 are the wino and bino mass parameters respectively, $\tan\beta$ is the ratio of the vacuum expectations of the two Higgs fields, M_A is the mass of pseudo-scalar Higgs boson, m_0 is the universal sfermion mass, A_b and A_t are the trilinear soft breaking parameters and the corresponding parameters for the first two generations are assumed zero.

We employ DarkSUSY to explore the parameter space of the phenomenological MSSM model [1]. The scan ranges of these parameters are: $50 \text{ GeV} < |\mu|, M_2, M_1, M_A, m_0 < 10 \text{ TeV}$, $1.1 < \tan\beta < 55$, $\text{sign}(\mu) = \pm 1$, $-3m_0 < A_t, A_b < 3m_0$. There are also other constraints from the theoretical consistency requirements and the accelerator data. Finally, we require the relic density of DM to be $\Omega_\chi h^2 < 0.128$ according to the 3σ upper limits of WMAP seven year results [4].

B. Density distribution

The most precise knowledge of the density profile of DM inside the halo comes from numerical simulations. Navarro et al. (1997) found that the density profile is universal for halos of different scales, referred as Navarro-Frenk-White (NFW) profile [5]

$$\rho(r) = \frac{\rho_s}{(r/r_s)(1+r/r_s)^2}, \quad (3)$$

where ρ_s and r_s are two scale parameters depending on the mass and concentration of the halo. However, due to the limit of resolution, some other density profiles with different central behavior were also proposed in literature. For example Moore et al. (1999) proposed the density profile with a much steeper inner slope [6]

$$\rho(r) = \frac{\rho_s}{(r/r_s)^{1.5} [1 + (r/r_s)^{1.5}]}. \quad (4)$$

The recent simulations tended to favor the Einasto profile with a gradual flattening of the logarithm slope of the inner behavior [7]. There were also studies showing that the density profile might be non-universal [8]. Considering the diversity of the inner profile of DM density distribution, we adopt NFW and Moore profiles for this study. The model parameters are $r_s = 20 \text{ kpc}$, $\rho_s = 0.35 \text{ GeV cm}^{-3}$ for NFW, and $r_s = 28 \text{ kpc}$, $\rho_s = 0.078 \text{ GeV cm}^{-3}$ for Moore profile respectively. The local density for these parameter sets is 0.4 GeV cm^{-3} .

To avoid the divergence of density when $r \rightarrow 0$, a cutoff scale is applied considering the fact that there should be a balance between the gravitational infall and the annihilation [9]. For common parameters of DM particle the maximum density is estimated to be $\sim 10^{18} \text{ M}_\odot \text{ kpc}^{-3}$ [10].

C. Substructures

The cosmological structures form hierarchically in the cold dark matter scenario, that is, the DM collapses to form small halos first, then grows to larger and larger halos through accretion and merger. Numerical simulations show that there are a large number of subhalos surviving the merger history and existing in the Milky Way dark matter halo [11–14]. The dwarf galaxies are a part of the Galactic subhalos which have been observed.

According to the simulations, the number density distribution of subhalos as a function of its mass and location can be parameterized as [15, 16]

$$\frac{dn}{dm_{\text{sub}} \cdot 4\pi r^2 dr} = \frac{n_0}{1 + (r/r_h)^2} \times \left(\frac{m_{\text{sub}}}{m_{\text{host}}} \right)^{-\alpha}, \quad (5)$$

with $r_h \approx 0.14 r_{\text{host}}$ for galaxy scale halo [16] and $\alpha \approx 1.9$ [15, 17]. The normalization n_0 is fixed by setting $N(> 10^8 \text{ M}_\odot) \approx 100$ (see [10] and references therein).

The density profile of each subhalo is also assumed to be NFW or Moore profile. To determine the density parameters of each subhalo, we use the concentration-mass relation given in Ref. [18]. The procedure of determining the parameters is as follows. For a halo with mass m_{sub} , the concentration is derived according to the $c_{\text{sub}}-m_{\text{sub}}$ relation. Then we have $r_s^{\text{NFW}} = r_{\text{sub}}/c_{\text{sub}}$ and $r_s^{\text{Moore}} = r_{\text{sub}}/0.63c_{\text{sub}}$ following the definition of concentration [18]. Finally ρ_s is determined by the subhalo mass.

To calculate the annihilation flux of photons from the subhalo population, we define the average density square as

$$\langle \rho_{\text{sub}}^2 \rangle(r) = \int dm_{\text{sub}} \frac{dn}{dm_{\text{sub}} \cdot 4\pi r^2 dr} \times \int_{V_{\text{sub}}} \rho_{\text{sub}}^2 dV, \quad (6)$$

where dV integrates over the volume of the subhalo. Replacing ρ^2 in $J(\psi)$ in Eq. (1) with $\langle \rho_{\text{sub}}^2 \rangle$ we calculate the photon flux from DM annihilation in the subhalos.

The $J(\psi)$ factor as a function of the angle ψ away from the GC direction is shown in Fig. 1. It can be seen that for the smooth halo the annihilation flux is highly concentrated in the GC. The substructure contribution is nearly isotropic in all directions. At large angles away from the GC the substructure component may dominate the annihilation flux for the Moore profile.

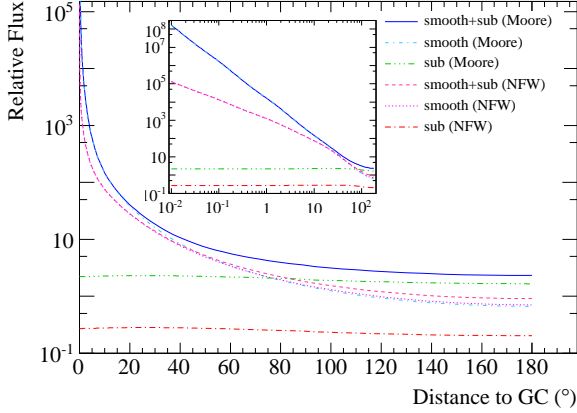


Figure 1: Angular distribution of DM annihilation luminosity (J factor) in the Milky Way. The inner plot uses log scale for x axis to show the details in the most central region.

III. DETECTABILITY ANALYSIS

A. Backgrounds

We first introduce the backgrounds which are essential for the detectability analysis of the DM-induced monochromatic γ -ray signal. The backgrounds include charged CR particles, such as all kinds of nuclei, electrons and positrons, and continuous γ -rays.

The CR nuclei and electrons/positrons can be rejected through the design of particle identification technique of the detector, however, there still are a few particles which may be misidentified as photons and form the background. The combined nuclei flux, mostly proton and Helium nuclei, can be written as [19]

$$\phi_n(E) = 1.49 \left(\frac{E}{\text{GeV}} \right)^{-2.74} \text{cm}^{-2}\text{s}^{-1}\text{sr}^{-1}\text{GeV}^{-1}, \quad (7)$$

which is an empirical formula from combined result of many measurements. For the electron plus positron spectrum, we adopt a broken power law parameterization

$$\begin{aligned} \phi_e(E) = & 1.5 \times 10^{-11} \left[1 + \left(\frac{E}{900 \text{ GeV}} \right)^{10/3} \right]^{-0.33} \\ & \times \left(\frac{E}{900 \text{ GeV}} \right)^{-3.0} \text{cm}^{-2}\text{s}^{-1}\text{sr}^{-1}\text{GeV}^{-1} \end{aligned} \quad (8)$$

according to the recent measurements by Fermi [20] and HESS [21, 22]. In the following we employ two efficiencies, η_n and η_e , to represent the rejection power of the charged CRs.

Then we come to the continuous γ -ray backgrounds. The first γ -ray background is the all-sky diffuse γ -ray emission, including Galactic and extra-galactic. For the extra-galactic γ -ray background we use the new measurement made by Fermi [23]

$$\phi_\gamma^{\text{extra}}(E) = 6.57 \times 10^{-7} \left(\frac{E}{\text{GeV}} \right)^{-2.4} \text{cm}^{-2}\text{s}^{-1}\text{sr}^{-1}\text{GeV}^{-1}. \quad (9)$$

The Fermi result of extra-galactic γ -ray emission is steeper than that obtained by EGRET [24], which will result in an order of magnitude lower background when extrapolating to high energies ($\sim \text{TeV}$).

Fermi collaboration also reported some data about the Galactic diffuse γ -ray emission (e.g., [23, 25, 26]), which is consistent with the results given by EGRET except the “GeV excess” [27]. Since the full Fermi data are unavailable at the present stage, we use the EGRET data about the Galactic diffuse γ -ray emission in this work. The Galactic diffuse γ -ray flux is parameterized as [28]

$$\phi_\gamma^{\text{galac}}(E) = N_0(l, b) \times 10^{-6} \left(\frac{E}{\text{GeV}} \right)^{-2.7} \text{cm}^{-2}\text{s}^{-1}\text{sr}^{-1}\text{GeV}^{-1}, \quad (10)$$

where

$$N_0 = \begin{cases} \frac{85.5}{\sqrt{1+(l/35)^2} \sqrt{1+(b/1.8)^2}} + 0.5 & |l| \leq 30^\circ \\ \frac{85.5}{\sqrt{1+(l/35)^2} \sqrt{1+[b/(1.1+0.022|l|)]^2}} + 0.5 & |l| > 30^\circ \end{cases}, \quad (11)$$

in which the galactic longitude l and latitude b are expressed in unit of degree. To make use of this measurement, we have to extrapolate Eq. (10) to higher energies.

Besides the diffuse γ -ray emission, there are additional sources in the GC region. Since the GC region is very important for DM searches, the γ -ray sources in the GC region are necessary to be paid more attention. HESS observation showed there was diffuse γ -ray emission in the region $|l| < 0.8^\circ$, $|b| < 0.3^\circ$ (GC ridge) on top of the diffuse background [29]. The spectrum is

$$\phi_{\gamma}^{\text{GC-diff}}(E) = 1.28 \times 10^{-4} \left(\frac{E}{\text{GeV}} \right)^{-2.29} \text{cm}^{-2}\text{s}^{-1}\text{sr}^{-1}\text{GeV}^{-1}. \quad (12)$$

Also there is at least one gamma-ray point source in the Galactic center area, which is labeled as 3EG J1746-2851 in EGRET catalog [30], HESS J1745-290 in HESS catalog [31] and 0FGL J1746.0-2900 in Fermi catalog [32]. The energy spectrum of this source given by HESS is [33]

$$\phi_{\gamma}^{\text{point}}(E) = 2.5 \times 10^{-7} \left(\frac{E}{\text{GeV}} \right)^{-2.21} \text{cm}^{-2}\text{s}^{-1}\text{GeV}^{-1}, \quad (13)$$

which is valid between 200 GeV and 10 TeV.

The differential fluxes of all the backgrounds mentioned above are plotted in Fig. 2. Here we show the results within the circle with 1 degree radius around the GC. The electron and nuclei fluxes are multiplied by factors 10^{-3} and 10^{-6} respectively, which represent the typical rejection power of a γ -ray detector. We can see that the largest background is the diffuse source and the point source in the GC region. The Galactic diffuse γ -ray emission is also important in the GC. However, for the sky regions far away from the GC, the extra-galactic background would also become import.

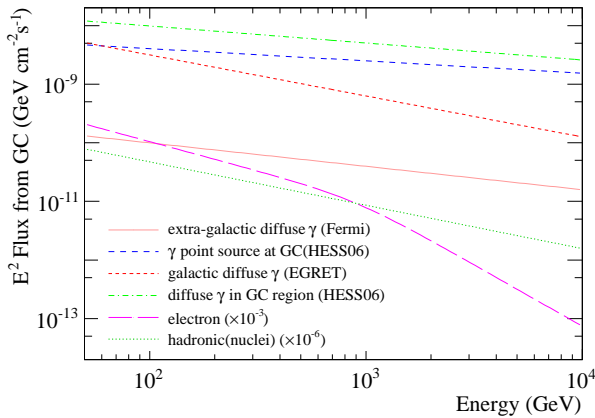


Figure 2: Spectra of the possible backgrounds from the 1 degree region around the GC.

B. Ideal detector

The sensitivity of monochromatic γ -ray detection is determined by the performance of a detector. First of

all, we need particle discrimination to reject most of the charged CRs, say nuclei and electrons/positrons. This can be done through charge detection, neutron detection and shower shape identification in calorimeter. The continuous γ -rays can be suppressed by improving the detector energy resolution. Furthermore, as can be seen in Fig. 1 the small region around the GC is the best candidate for the line spectrum γ -rays detection. Thus good angular resolution will also be effective to increase the signal-to-noise ratio.

To simplify the study, we characterize the detector with some static parameters of the performance, that is, the parameters don't change with incident energy, direction, or particle type, like the energy resolution, the angular resolution, the field of view, the rejection power of electrons and nuclei and so on. The effective area of detector and exposure time are also key factors of the detection, however, the overall performance can be easily scaled given different effective area and exposure time. With the results of ideal detectors, we can provide the requirement of a real detector.

C. Sensitivity calculation

The event counts on a detector can be written as

$$N_i = \eta_i \cdot T_{\text{eff}} \cdot A \cdot f_i, \quad (14)$$

where η_i is the detection efficiency of incident particle, usually assumed to be 90% for photon, and equal to the rejection power for electron and nuclei, T_{eff} is the effective exposure time for a given source or small sky region, A is the active area of detector, and f_i is the flux of signal or background in given energy range and sky region. For a detector with energy resolution σ_e , f_i can be derived according to the differential flux ϕ

$$f_i = \int_{\Delta\Omega} d\Omega \int_{E_{\gamma}-3\sigma_E}^{E_{\gamma}+3\sigma_E} dE \phi_i(E, l, b). \quad (15)$$

Here we choose the energy window to be $\pm 3\sigma_E$ around E_{γ} , and $\Delta\Omega$ refers to the chosen observation field. Note for point source the above integral with respect to Ω disappears.

The detection significance is defined as $S = N_s / \sqrt{N_b}$ with N_s the count of signal and N_b the count of background. The sensitivity can be derived as the minimal signal flux needed for a detection significance $S = 5$.

IV. GC REGION SENSITIVITY WITH ANALYTICAL ESTIMATE

In this section we estimate the sensitivity of monochromatic γ -ray detection from the GC region by DM annihilation. We choose a typical planar calorimeter type detector with $1\text{m} \times 1\text{m}$ size. With one year of flight on the orbit of International Space Station (ISS) and the

assumption of 90 degree field of view, the effective exposure time is $\sim 7.9 \times 10^6 s$, which is about 1/4 of one year. More detail of effective exposure time can be found in Fig. 6.

The background event number is

$$\begin{aligned}
 N_b &= N_{\text{galac}} + N_{\text{extra}} + N_e + N_n + N_{\text{point}} + N_{\text{GC-diff}} \\
 &= T_{\text{eff}} A \int_{E_\gamma - 3\sigma_E}^{E_\gamma + 3\sigma_E} dE \\
 &\quad \times \left[\int_{\Delta\Omega} d\Omega \eta \phi_\gamma^{\text{galac}}(E) \right. \\
 &\quad + \Delta\Omega (\eta \phi_\gamma^{\text{extra}}(E) + \eta_e \phi_e(E) + \eta_n \phi_n(E)) \\
 &\quad \left. + \eta \phi_\gamma^{\text{point}}(E) + \eta \Omega_{\text{GC ridge}} \phi_\gamma^{\text{GC-diff}}(E) \right], \quad (16)
 \end{aligned}$$

where $\Delta\Omega = \pi(\sigma_d + 1)^2 \times (\pi/180)^2$ is the solid angle considered for event direction selection, in order to keep the same number of signal events, where σ_d is the detector resolution angle in unit of degree. Another method of events direction selection is to keep events of 1° from GC after point spreading of detector angle resolution. Considering that the largest backgrounds come from point-like sources from GC, and they expands the same as the cuspy Moore dark matter profile, the one-degree selection after expansion would result in same level of decreasing of both signal and background events number, which means poorer sensitivity. On the other hand, if we select events with larger radius, we can keep basically the same number of signal events, and better sensitivity. Therefore the minimal monochromatic photon flux from DM annihilation within ~ 1 degree around the GC is $f_{\text{min}} = 5\sqrt{N_b}/\eta T_{\text{eff}} A$, for a 5σ detection.

The results of f_{min} for different detector performance, i.e., different energy resolution, angular resolution, electron rejection and nuclei rejection respectively, are shown in Fig. 3. The default detector performance settings are: energy resolution 1.5%, angular resolution 0.5° , electron rejection 10^{-4} and nuclei rejection 10^{-7} . The different performances used in the calculation are summarized in Table I on page 5. The dots and triangles in the figure are the MSSM model predictions with a random scan in the eight-dimensional parameter space as introduced in Sec. II A. Both Moore and NFW profile are calculated and plotted. It is shown that the default detector configuration is powerful enough to probe much of the MSSM parameter space for the model with DM density as cuspy as Moore type. If the DM density profile is NFW-like the sensitivity will be worse. We will discuss the effects of different density profiles more in the following.

In Fig. 4 we show the comparison of sensitivities for longer exposure and larger area of the same type detector. The upper limits of monochromatic photons from 30 to 200 GeV derived according to 11 month Fermi data are shown by the line with errorbars [34]. Note the observation region of Fermi's result is $|b| > 10^\circ$ plus $20^\circ \times 20^\circ$ area around the GC, which is much larger than 1 degree around GC adopted here. Therefore the limits from GC

Table I: GC detectability calculation configuration

common setup	detector area: 1 m^2 , exposure time: $7.9 \times 10^6 \text{ s}$, energy range: $50 \text{ GeV} \sim 10 \text{ TeV}$
energy resolution	1%, 1.5%, 2%, 5%, 10%
angular resolution	0.1° , 0.3° , 0.5° , 1.0° , 3.0°
electron rejection	10^0 , 10^{-1} , 10^{-2} , 10^{-3} , 10^{-4}
proton rejection	10^{-2} , 10^{-3} , 10^{-4} , 10^{-5} , 10^{-7}

would be smaller than the present given values. We just plot the results here for reference.

In Fig. 5 the minimal detectable cross section is shown, for $\gamma\gamma$ (left) and γZ_0 (right) channels respectively. In this plot the default detector performance is adopted, and we show the results for the NFW and Moore profiles, with different sky regions. It is shown that for the NFW profile the detectability will be orders of magnitude worse than that for the Moore profile. We also note that for the NFW profile the sensitivity is not affected significantly by the choice of sky area if the GC is included. However, it is not the case for the Moore profile. This can be understood that for the Moore profile the signal flux drops very fast with the increase of the angle to the GC, which leads to a fast decrease of the signal-to-noise ratio. Therefore the large-angle average results in a worse sensitivity than the case focusing on the small region around the GC. The 95% exclusion limits of the cross section for the NFW profile from Fermi are also plotted [34]. To compare with the capability of Fermi, we show the exclusion power of the detector with the default parameters mentioned before, at 1σ level for the same density profile and observational sky region as Fermi.

V. WHOLE SKY SCAN SENSITIVITY WITH MONTE-CARLO SIMULATION

In this section we discuss the all-sky observation with scan mode. The effective exposure time is non-uniform at different directions for specific orbit of the detector. Therefore the simple analytical method discussed in the previous section does not work any more. We turn to use fast Monte-Carlo method to simulate the counts of signal and background, and calculate the sensitivity.

A. Simulation configuration

The flight orbit is assumed to be the orbit of ISS. We put an ideal detector on the orbit, and calculate the signal and background particle counts by the Monte-Carlo sampling. We take the orbit data of ISS in 2003 as an example. The orbit of ISS has not changed too much in the period of several years. The sky-map of exposure time is plotted in Fig. 6.

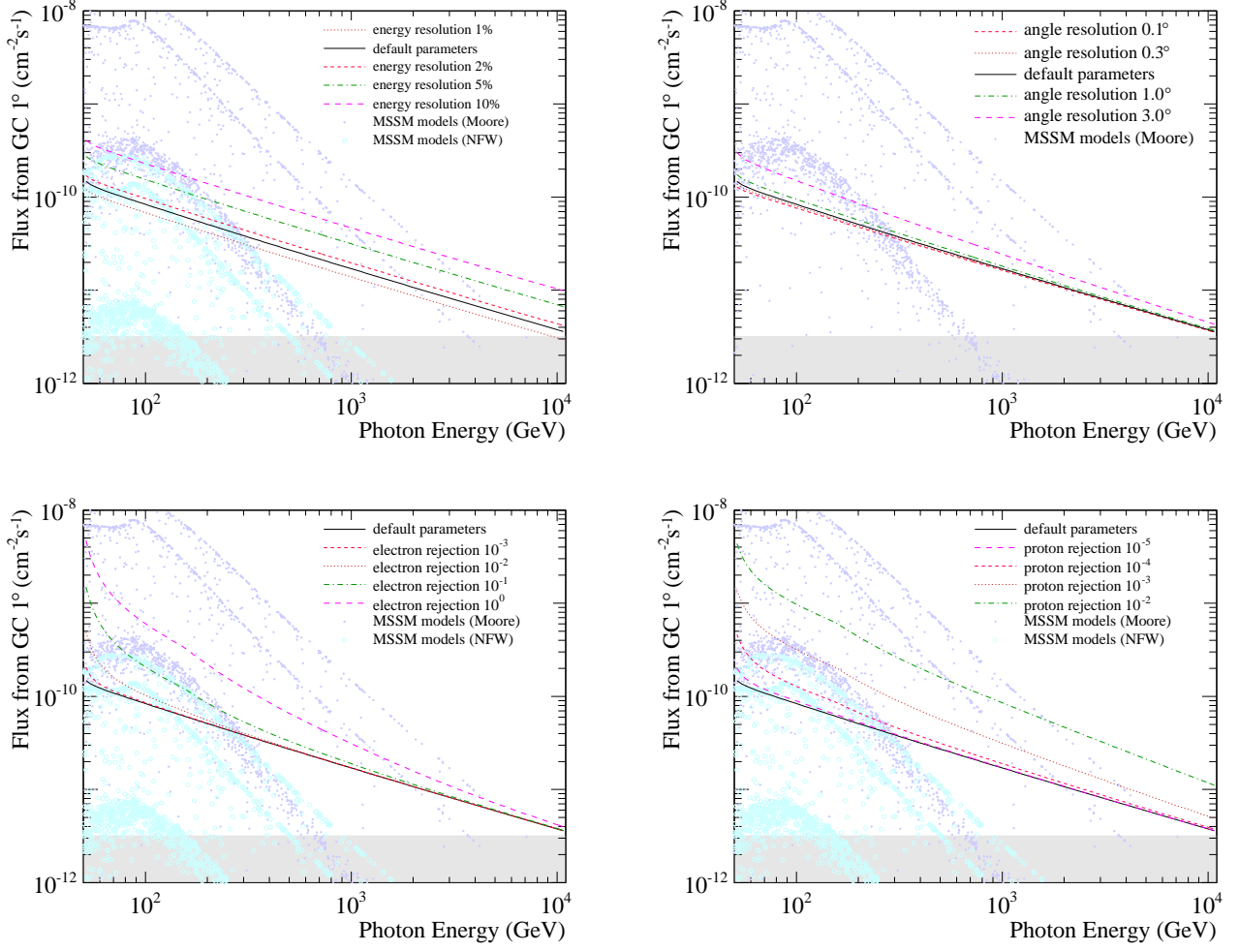


Figure 3: The sensitivity with different detector features: energy resolution (top-left), angular resolution (top-right), electron rejection (bottom-left), nuclei rejection (bottom-right). The default settings are: energy resolution 1.5%, angular resolution 0.5° , electron rejection 10^{-4} and nuclei rejection 10^{-7} . The gray area at the bottom of each panel represents the flux corresponding to less than one event per year (exposure time) for a 1 m^2 detector.

We choose detectors with a series of property parameters, including energy resolution, field of view, electron and nuclei rejection powers. Seven neutralino masses, between 50 GeV and 1200 GeV, are chosen in the simulation. The details of the configurations are listed in Table II.

Table II: Survey simulation configuration

common configuration	geometry factor: $3.14 \text{ m}^2 \text{sr}$, flight time: 1 year, flight orbit: ISS orbit
simulated energy (GeV)	77.6, 199.7, 416.3, 611.4, 808.6, 1006.0, 1220.9
energy resolution	1%, 1.5%, 2%
field of view	40° , 60° , 90°
electron rejection	10^{-2} , 10^{-3} , 10^{-4}
proton rejection	10^{-5} , 10^{-6} , 10^{-7}

To get better statistics, a large enough cross section was chosen in the simulation. The photons from $\gamma\gamma$ and γZ_0 annihilation channels are not distinguished, and only a sensitivity for single gamma line emission was given. Actually the photons from these two channels can not be discriminated when neutralino mass is larger than several hundred GeV, and if neutralino mass is small, there could be two peaks on the photon energy spectrum, thus the sensitivity would be higher.

The overall contribution from DM annihilation, not only the smooth halo, but also the substructures, is taken into account. In the simulation we use Moore profile for both the smooth halo and subhalos. To compare with theory predictions, the model points are plotted along with the minimum detectable curves. In the calculation both Moore and NFW profile are used. And also the contribution of substructures and smooth halo are summed together.

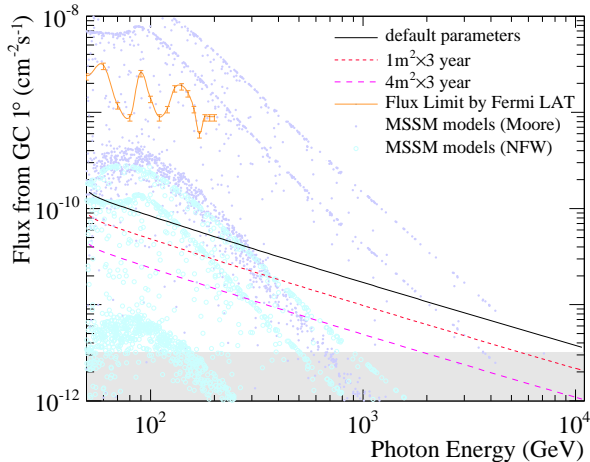


Figure 4: The sensitivity with different exposure factor and detector area.

B. Event generation and reconstruction simulation

The basic procedure of the simulation can be divided into two phases. First is the generation of the event samples according to the angular and energy distributions of each component, including the signal and backgrounds. The second phase is to simulate the event reconstruct process based on the detector performances.

For the signal events, the energy of generated photon is monochromatic for a given neutralino mass. The spatial distribution follows the result as shown in Fig. 1. The energy spectra and angular distributions of backgrounds are described in Sec. III A. In the simulation, we also need to know the direction of the detector. The detector pointing direction is set to be the same as the direction of ISS.

The events are generated in interval of one second in detector operation time. To simplify the simulation code, static event rate for each component is used. The event rate is set to be the maximum value that can be received by the detector with acceptance $4\pi \cdot A$, for energy range from 30 GeV to 1400 GeV, and a Poisson smear is used when event number in the one-second-interval is too small. However, the actual events received by a specific detector will be much smaller than the above value since the effective area for photons with large incident angle will decrease. This effect is taken into account at the second phase through an efficiency factor η , defined as $\eta_i \cos(p)$ when $p < p_{FOV}$, and 0 when $p \geq p_{FOV}$, where p is the angle between the incident photon and the detector pointing direction, p_{FOV} is the maximum receiving angle of incident particles, and η_i is the selection efficiency for different incident particle. For photons the selection efficiency usually assumed to be 90%. For electrons and nuclei events, the detector rejection power is used as the selection efficiency. Then one event is kept

with probability η .

The events kept in the efficiency selection are then reconstructed. The reconstruction of energy is simply implemented by a Gaussian smear of the inject photon energy. The Gaussian width is σ_e , which represents the energy resolution of the detector. The nuclei rejection and electron rejection are simulated as a fixed pass rate as mentioned before. Passed electrons and nuclei are reconstructed the same way as photons. Figure 7 on page 8 shows a sample reconstructed energy spectrum for the neutralino mass 416 GeV. The direction reconstruction simulation is in the same way as energy reconstruction, with two-dimensional Gaussian smear.

C. Results of simulation

The results of sensitivities for scan observation are shown in Fig. 8, for different detector performance. The area of detector is adopted to be 1 m \times 1 m. The points represent the MSSM model predicted fluxes of the all-sky DM annihilation, with substructures included, for both Moore and NFW profile. Compared with the results of GC, the scan mode will be less sensitive for detecting the DM annihilation signal by more than one order of magnitude.

VI. DISCUSSION AND CONCLUSION

In this work we studied the strategy and feasibility of the monochromatic γ -ray detection from DM annihilation. We studied the detectability of the monochromatic γ -rays from the GC and from the dark matter halo and subhalos, by analytical analysis and numerical Monte-Carlo simulation. The detector performance is studied for the purpose of monochromatic γ -ray detection.

The sensitivity depends on the observation region and the DM density profiles. According to the Moore profile, the sensitivity of GC region would be much higher than other region. However, this is not true for NFW-like profiles. As we currently have little knowledge about the actual distribution, we can not rely on a particular model. Until now, high energy gamma observations, such as HESS and Fermi, have not seen any evidence in the GC region. A safe strategy could be starting from the scan mode, then focusing on the interesting area if any evidence is found. On the other hand, the GC is always an interesting region for possible DM signals. The observation of the GC should be tuned as much as possible.

In order to detect the monochromatic γ -ray emission of DM annihilation in scan mode, the energy resolution and geometry factor, both detector area and field of view, are the most important detector feature. However, The resources are usually very limited on orbit, on both detector mass and power supply. With a given mass of the detector, thinner calorimeter would lead to larger active area. On the other hand, thinner calorimeters usually

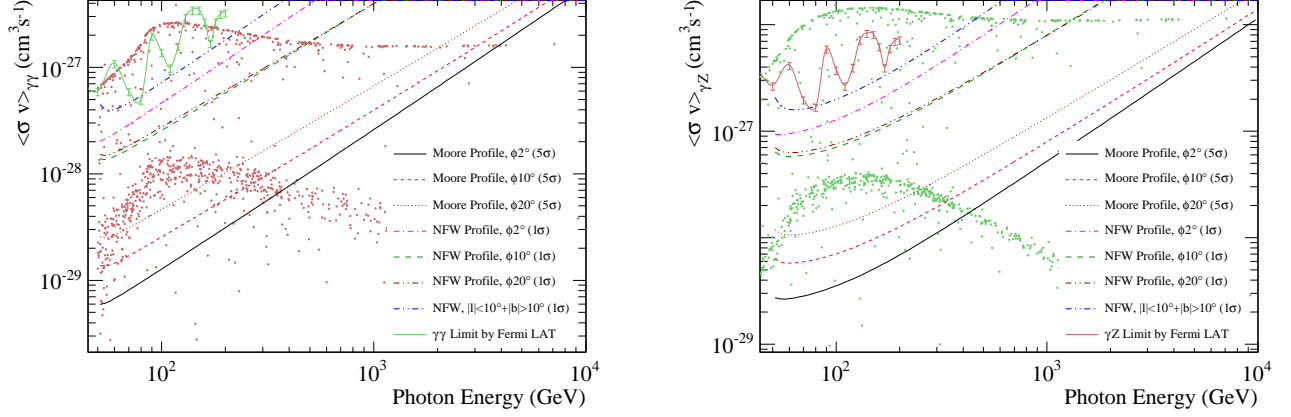


Figure 5: The minimal detectable cross section for $\gamma\gamma$ (left) and γZ_0 (right) channels in different observation area

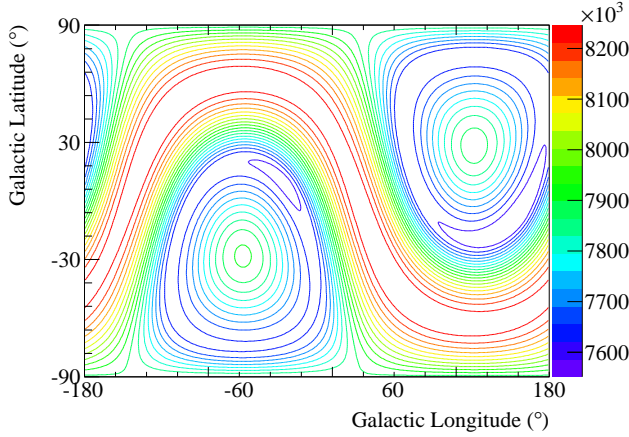


Figure 6: Sky-map of effective exposure time according to the 2003 ISS orbit data. The whole sky area is divided into 360×180 cells, with $1^\circ \times 1^\circ$ of each cell. This map is derived as follows. The effective exposure time of each cell is calculated as $\cos(\theta)$ where θ is the angle between the direction of the ISS and the direction of the cell. If $\theta > \pi$ the effective exposure time is set to zero. Then the effective time of each cell is calculated in an interval of one second, and accumulated for all the time in one year (3.15×10^7 s).

have poorer energy resolution. Therefore, to get better sensitivity, a careful balance is needed in detector designing. Also any detector design that would limit the field of view of the detector should better be avoided. At low energies (< 300 GeV), the ability to reject cosmic-ray background, electrons and nuclei, are also important. To keep cosmic-ray background low enough, that is, lower than the major background, diffuse γ , at least 10^{-3} electron rejection and 10^{-6} proton rejection is required.

If we are focusing on GC or other interesting region in pointing mode, the angular resolution, instead of field of view, becomes very important. In the GC region, the γ -

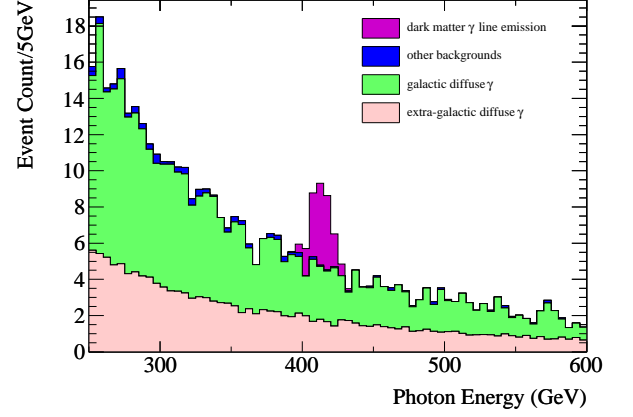


Figure 7: A sample reconstructed stacked photon energy spectrum, for neutralino mass 416 GeV.

ray emission is complex: several point sources exist there. Thus good angular resolution is needed to separate them apart, and suppress these point source backgrounds. Of course the energy resolution and detector area are still important features in order to detect monochromatic γ -rays. Also, at low energy, the rejection power requirements of electron and proton are the same as in scan mode.

Acknowledgments

This work is supported by Natural Sciences Foundation of China (No. 10435070, No. 10773011, No. 10721140381, No. 10099630) and by China Ministry of Science and Technology (No. 2007CB16101, No. 2010CB833000).

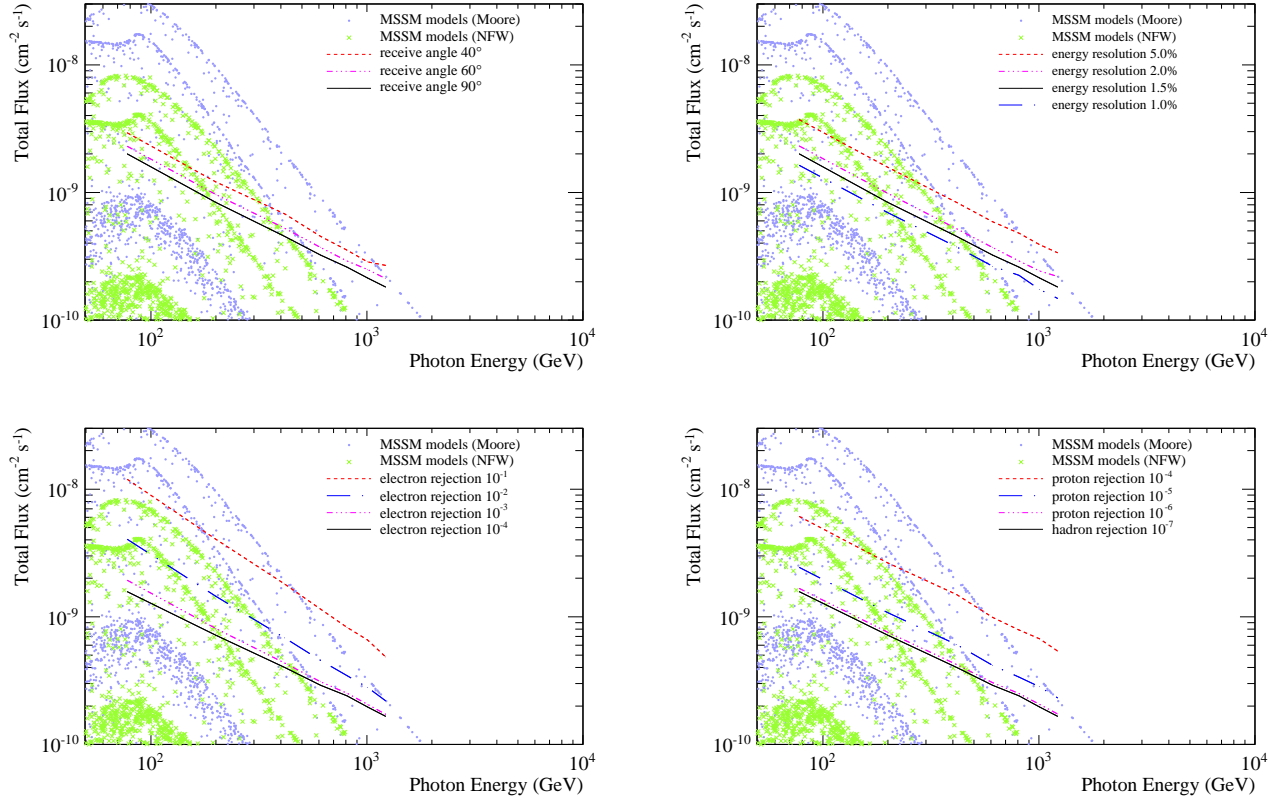


Figure 8: The minimum detectable flux of DM line emission in scan mode. Top-left: comparison among different maximum receiving angle (field of view); top-right: comparison among different energy resolution; bottom-left: comparison among different electron rejection power; bottom-right: comparison among different nuclei rejection power. The default parameters are energy resolution 1.5%, maximum receiving angle 90° , electron rejection 10^{-4} , and proton rejection 10^{-7} .

-
- [1] P. Gondolo, J. Edsjö, P. Ullio, L. Bergström, M. Schelke, and E. A. Baltz, *Journal of Cosmology and Astro-Particle Physics* **7**, 8 (2004), arXiv:astro-ph/0406204.
- [2] R. Catena and P. Ullio, *ArXiv e-prints* (2009), 0907.0018.
- [3] P. Salucci, F. Nesti, G. Gentile, and C. F. Martins, *ArXiv e-prints* (2010), 1003.3101.
- [4] E. Komatsu, K. M. Smith, J. Dunkley, C. L. Bennett, B. Gold, G. Hinshaw, N. Jarosik, D. Larson, M. R. Nolte, L. Page, et al., *ArXiv e-prints* (2010), 1001.4538.
- [5] J. F. Navarro, C. S. Frenk, and S. D. M. White, *Astrophys. J.* **490**, 493 (1997), arXiv:astro-ph/9611107.
- [6] B. Moore, T. Quinn, F. Governato, J. Stadel, and G. Lake, *Mon. Not. Roy. Astron. Soc.* **310**, 1147 (1999), arXiv:astro-ph/9903164.
- [7] J. F. Navarro, A. Ludlow, V. Springel, J. Wang, M. Vogelsberger, S. D. M. White, A. Jenkins, C. S. Frenk, and A. Helmi, *Mon. Not. Roy. Astron. Soc.* **402**, 21 (2010), 0810.1522.
- [8] Y. P. Jing and Y. Suto, *Astrophys. J. Lett.* **529**, L69 (2000), arXiv:astro-ph/9909478.
- [9] V. S. Berezinsky, A. V. Gurevich, and K. P. Zybin, *Physics Letters B* **294**, 221 (1992).
- [10] J. Lavalle, Q. Yuan, D. Maurin, and X. Bi, *Astron. Astrophys.* **479**, 427 (2008), 0709.3634.
- [11] G. Tormen, A. Diaferio, and D. Syer, *Mon. Not. Roy. Astron. Soc.* **299**, 728 (1998), arXiv:astro-ph/9712222.
- [12] B. Moore, S. Ghigna, F. Governato, G. Lake, T. Quinn, J. Stadel, and P. Tozzi, *Astrophys. J. Lett.* **524**, L19 (1999), arXiv:astro-ph/9907411.
- [13] S. Ghigna, B. Moore, F. Governato, G. Lake, T. Quinn, and J. Stadel, *Astrophys. J.* **544**, 616 (2000), arXiv:astro-ph/9910166.
- [14] A. R. Zentner and J. S. Bullock, *Astrophys. J.* **598**, 49 (2003), arXiv:astro-ph/0304292.
- [15] L. Gao, S. D. M. White, A. Jenkins, F. Stoehr, and V. Springel, *Mon. Not. Roy. Astron. Soc.* **355**, 819 (2004), arXiv:astro-ph/0404589.
- [16] J. Diemand, B. Moore, and J. Stadel, *Mon. Not. Roy. Astron. Soc.* **352**, 535 (2004), arXiv:astro-ph/0402160.
- [17] V. Springel, J. Wang, M. Vogelsberger, A. Ludlow, A. Jenkins, A. Helmi, J. F. Navarro, C. S. Frenk, and S. D. M. White, *Mon. Not. Roy. Astron. Soc.* **391**, 1685 (2008), 0809.0898.
- [18] J. S. Bullock, T. S. Kolatt, Y. Sigad, R. S. Somerville, A. V. Kravtsov, A. A. Klypin, J. R. Primack, and A. Dekel, *Mon. Not. Roy. Astron. Soc.* **321**, 559 (2001),

- arXiv:astro-ph/9908159.
- [19] T. K. Gaissler, M. Honda, P. Lipari, and T. Stanev, in *International Cosmic Ray Conference* (2001), vol. 5 of *International Cosmic Ray Conference*, pp. 1643–+.
 - [20] A. A. Abdo, M. Ackermann, M. Ajello, W. B. Atwood, M. Axelsson, L. Baldini, J. Ballet, G. Barbiellini, D. Bastieri, M. Battelino, et al., *Physical Review Letters* **102**, 181101 (2009), 0905.0025.
 - [21] F. Aharonian, A. G. Akhperjanian, U. Barres de Almeida, A. R. Bazer-Bachi, Y. Becherini, B. Behera, W. Benbow, K. Bernlöhr, C. Boisson, A. Bochow, et al., *Physical Review Letters* **101**, 261104 (2008), 0811.3894.
 - [22] F. Aharonian, A. G. Akhperjanian, G. Anton, U. Barres de Almeida, A. R. Bazer-Bachi, Y. Becherini, B. Behera, K. Bernlöhr, A. Bochow, C. Boisson, et al., *Astron. Astrophys.* **508**, 561 (2009).
 - [23] A. A. Abdo, M. Ackermann, M. Ajello, W. B. Atwood, L. Baldini, J. Ballet, G. Barbiellini, D. Bastieri, B. M. Baughman, K. Bechtol, et al., *Physical Review Letters* **104**, 101101 (2010), 1002.3603.
 - [24] P. Sreekumar, D. L. Bertsch, B. L. Dingus, J. A. Esposito, C. E. Fichtel, R. C. Hartman, S. D. Hunter, G. Kanbach, D. A. Kniffen, Y. C. Lin, et al., *Astrophys. J.* **494**, 523 (1998), arXiv:astro-ph/9709257.
 - [25] A. A. Abdo, M. Ackermann, M. Ajello, W. B. Atwood, M. Axelsson, L. Baldini, J. Ballet, G. Barbiellini, D. Bastieri, B. M. Baughman, et al., *Astrophys. J.* **703**, 1249 (2009), 0908.1171.
 - [26] A. A. Abdo, M. Ackermann, M. Ajello, B. Anderson, W. B. Atwood, M. Axelsson, L. Baldini, J. Ballet, G. Barbiellini, D. Bastieri, et al., *Physical Review Letters* **103**, 251101 (2009), 0912.0973.
 - [27] S. D. Hunter, D. L. Bertsch, J. R. Catelli, T. M. Dame, S. W. Digel, B. L. Dingus, J. A. Esposito, C. E. Fichtel, R. C. Hartman, G. Kanbach, et al., *Astrophys. J.* **481**, 205 (1997).
 - [28] L. Bergström, P. Ullio, and J. H. Buckley, *Astroparticle Physics* **9**, 137 (1998), arXiv:astro-ph/9712318.
 - [29] F. Aharonian, A. G. Akhperjanian, A. R. Bazer-Bachi, M. Beilicke, W. Benbow, D. Berge, K. Bernlöhr, C. Boisson, O. Bolz, V. Borrel, et al., *Nature* **439**, 695 (2006), arXiv:astro-ph/0603021.
 - [30] H. A. Mayer-Hasselwander, D. L. Bertsch, B. L. Dingus, A. Eckart, J. A. Esposito, R. Genzel, R. C. Hartman, S. D. Hunter, G. Kanbach, D. A. Kniffen, et al., *Astron. Astrophys.* **335**, 161 (1998).
 - [31] F. Aharonian, A. G. Akhperjanian, A. R. Bazer-Bachi, M. Beilicke, W. Benbow, D. Berge, K. Bernlöhr, C. Boisson, O. Bolz, V. Borrel, et al., *Physical Review Letters* **97**, 221102 (2006), arXiv:astro-ph/0610509.
 - [32] A. A. Abdo, M. Ackermann, M. Ajello, W. B. Atwood, M. Axelsson, L. Baldini, J. Ballet, D. L. Band, G. Barbiellini, D. Bastieri, et al., *Astrophys. J. Supp.* **183**, 46 (2009), 0902.1340.
 - [33] F. Aharonian, A. G. Akhperjanian, G. Anton, U. Barres de Almeida, A. R. Bazer-Bachi, Y. Becherini, B. Behera, K. Bernlöhr, C. Boisson, A. Bochow, et al., *Astron. Astrophys.* **503**, 817 (2009), 0906.1247.
 - [34] A. A. Abdo, M. Ackermann, M. Ajello, W. B. Atwood, L. Baldini, J. Ballet, G. Barbiellini, D. Bastieri, K. Bechtol, R. Bellazzini, et al., *Physical Review Letters* **104**, 091302 (2010), 1001.4836.